Passivation of CdS/Cu₂ZnSnS₄ Interface from Surface Treatments of Kesterite-Based Thin-Film Solar Cells

Natalia M. Martin,* Charlotte Platzer-Björkman, Konstantin Simonov, Håkan Rensmo, and Tobias Törndahl

Surface treatments of Cu_2ZnSnS_4 have shown a beneficial effect on the solar cells performance due to a reduction in the open-circuit voltage (V_{OC}) deficit. Several reasons have been suggested for the V_{OC} deficit, including an unfavorable band alignment at the buffer/Cu_2ZnSnS_4 interface. Herein, the influence of Cu_2ZnSnS_4 surface treatment (air exposure and air anneal) on the electronic and chemical properties of Cu_2ZnSnS_4 and CdS/Cu_2ZnSnS_4 interfaces is investigated. Using hard X-ray photoelectron spectroscopy, it is shown that the band alignment at the CdS/Cu_2ZnSnS_4 interface is not significantly altered by the applied surface treatment. The device enhancement is instead connected to interface passivation for the surface-treated Cu_2ZnSnS_4 samples due to the formation of SnO_x which is shown to not be fully removed upon KCN etching prior to the buffer layer deposition. In addition, a surface treatment of the Cu_2ZnSnS_4 absorber prior to buffer layer deposition influences the growth of CdS buffer, as a thicker CdS-overlayer is observed to grow on a surface-treated Cu_2ZnSnS_4 sample as compared with a nontreated sample. This suggests that a reoptimization of the CdS thickness for a given Cu_2ZnSnS_4 surface treatment is required.

1. Introduction

Sulfide kesterite Cu_2ZnSnS_4 (CZTS) is considered as a promising absorption layer material in next-generation thin-film solar cells due to the earth-abundant component elements being also nontoxic and environmentally friendly. However, the efficiency is still far below the theoretical limit and below that of other types of solar cells containing less abundant and toxic elements.[1] It is well known that the performance of kesterite thin-film solar cells depends strongly on the atomic structure and chemical composition of the CZTS absorber layer and adjacent interfaces; yet, the full understanding of such interfaces is missing mainly because of the difficulty to investigate buried interfaces directly and nondestructively using conventional techniques. Hard X-ray photoelectron spectroscopy (HAXPES) offers a suitable solution. Due to higher inelastic mean free paths of photoemitted electrons at high kinetic energies as compared with conventional X-ray photoelectron spectroscopy (XPS), HAXPES is an important tool to provide information on the structural, chemical, and electronic properties on different depths and of buried interfaces of a thin-film solar cell layer stack. Tajima et al. showed that HAXPES can successfully be used to directly measure the valence band offset (VBO) at the CdS/CZTS interface.[2]

A surface treatment consisting of either air annealing or air exposure, and applied prior to buffer layer deposition, has been shown to improve the performance of both sulfide or selenide CZTS(Se)-based thin-film solar cells.[3–7] An increase in the open-circuit voltage (V_{OC}) has also been reported for the air anneal treatment,[3] where unfavorable band alignment at the buffer/absorber interface may be one of the factors limiting the V_{OC}.[8] Still, only little is known about how different surface treatments affect the chemical and electronic properties of CZTS(Se) absorbers and the subsequent deposition of different buffers. Previous works have suggested the passivation of grain boundaries,[4] modification of surface composition,[9] or even a bandgap widening as possible effects of air annealing of CZTS(Se).[10] In particular, some studies show that the presence of SnO_x at the grain boundaries in polycrystalline CZTSSe solar cells, formed after annealing the bare absorber in air, correlates with high device performance and is proposed to passivate grain boundary recombination sites.[4] Most works on surface treatments of kesterite solar cells were carried out on CZTSSe or CZTSe. Even though it is expected that CZTS would behave similarly to CZTSe, a full understanding of the effect of CZTS

Dr. N. M. Martin, Prof. C. Platzer-Björkman, Prof. T. Törndahl
Solar Cell Technology
Department of Materials Science and Engineering
Uppsala University
SE-751 21 Uppsala, Sweden
E-mail: Natalia.Martin@angstrom.uu.se

Dr. K. Simonov, Prof. H. Rensmo
Molecular and Condensed Matter
Department of Physics and Astronomy
Uppsala University
SE-751 21 Uppsala, Sweden

Dr. K. Simonov
Department of Materials and Process Development
Swerim AB
Box 7047, SE-164 07 Kista, Sweden

surface treatment prior to buffer layer deposition and its influence on the buffer layer growth is missing.

Moreover, the potassium cyanide (KCN) etch treatment used prior to a buffer layer deposition step is generally used as a procedure to selectively etch conductive CuS_x phases and clean air-exposed (AE) absorber surfaces. Such a treatment shall, in principle, remove most of the contaminants (including oxides and secondary phases) and may change the surface composition.[11]

The aim of this study is to compare different surface treatments (air exposure and air annealing) of sulfide CZTS and their influence on the interface with CdS buffer after they have been etched by KCN. A comparison with a nontreated (fresh) surface is also included. For this task, XPS measurements in both soft and hard X-ray regimes (XPS and HAXPES) were used to non-destructively study the chemical and electronic properties of the treated CZTS surface and the CdS/CZTS interface region.

Current–voltage and quantum efficiency measurements were used to correlate the structural and chemical findings from the photoelectron spectroscopy measurements with the device characteristics.

2. Experimental Section

2.1. Sample Preparation and Device Characterization

The CZTS samples were prepared by sputtering Cu–Zn–Sn–S precursors from CuS, ZnS, and SnS targets on a 300 nm Mo-coated soda lime glass (SLG) substrate in an argon atmosphere. The bulk composition of the precursors measured by X-ray fluorescence showed composition ratios of Cu/Sn = 1.89 and Zn/(Cu + Sn) = 0.36, typical for this type of solar cells. After deposition, the precursors were sulfurized for 13 min at 585 °C in a pyrolytic carbon-coated graphite box containing 250 mg of elemental sulfur, as described further in the study by Larsen et al.[12] After sulfurization, the samples were exposed to different surface treatments, as shown in **Table 1**, and described in the following paragraphs. For the first set of samples (F), the direct deposition of the buffer layer took place after a short air exposure (<10 min). For the second set of samples, air exposure for 24 h at atmospheric pressure and room temperature conditions in the clean room environment was applied (AE). The third set of samples were exposed to an air-annealed (AA) treatment by placing the samples onto a preheated hot plate set to 300 °C for 80 s followed by a similar annealing at 200 °C for 10 min. After the air annealing, the samples were removed from the hot plate and cooled to room temperature. All samples (sets 1–3) were etched in 5% potassium cyanide (KCN) (2 min

Table 1. Summary of the applied surface treatments for the investigated samples.

Sample ID	Surface treatment
F	No treatment, freshly prepared CZTS
AE	24 h air exposure of CZTS in clean room environment
AA	Air annealing of CZTS on a hot plate at 300 °C (80 s) + 200 °C (10 min)

in 1.5 M aqueous solution at room temperature, followed by an H_2O rinse) prior to buffer layer deposition. The CdS was deposited by a chemical bath deposition (CBD) process, in a bath of cadmium sulfate, thiourea, and aqueous ammonia, at 60 °C for 2 min 30 s resulting in a thin CdS layer. The deposition time was chosen based on previous investigations on CdS deposition time using this process, and aiming for around 5–10 nm films. A longer deposition time of 8 min 15 s, which is the standard deposition time used in our baseline CdS deposition[13] resulting in a CdS thickness of ≈50 nm, was used to grow a thicker CdS reference sample.

The as prepared buffer/absorber samples described earlier were sealed in a plastic bag under N_2 and transported to the synchrotron for characterization. At the beamline, the samples were briefly exposed to air while being mounted on the sample holder and then transferred into the ultra high vacuum system. The exposure time of the samples (<15 min) to the ambient atmosphere was similar to that in the fabrication process of CZTS devices in our laboratory, which minimized the chemical difference between the investigated samples and solar cell devices.

One half of each sample was later processed into devices by sputter deposition of an i-ZnO/ZnO:Al bilayer and mechanical scribing to define cells with an area of 0.05 cm². Dark and illuminated current–voltage measurements were carried out using a Newport IV ABA solar simulator. External quantum efficiency measurements to determine the bulk bandgap were carried out using a homebuilt setup. The relative composition of the CZTS films was analyzed by X-ray fluorescence spectroscopy (XRF) using a Panalytical Epsilon 5 EDXRF spectrometer.

2.1.1. X-ray Photoelectron Spectroscopy

XPS measurements including core-level spectroscopy and valence band (VB) spectroscopy were conducted using both a lab-based X-ray source and higher photon energies at the synchrotron to monitor the composition, chemical state, and electronic structure of CZTS-based solar cells. The XPS measurements were carried out both after the KCN etching of the treated absorbers (using lab-based XPS to investigate the state of the surface before buffer layer deposition) and after buffer layer deposition (using HAXPES to investigate the buffer/absorber interface).

Lab-based XPS measurements were carried out using a PHI Quantera II scanning XPS microprobe with monochromatized Al Kα (1486.6 eV) and a beam diameter of 100 μm. The base pressure in the analysis chamber was about 1×10^{-9} mbar during the measurements. Pass energies of 224 and 55 eV with dwell times of 0.05 s point^{-1} were used to collect the survey and detail spectra, respectively.

Synchrotron-based HAXPES measurements were carried out at the GALAXIES undulator beamline of the Soleil synchrotron (France).[14] The spectra were recorded using a VG Scienta EW4000 energy electron analyser at normal emission and excitation energies $hv = 3$ and $hv = 9$ keV, respectively. The beamline, equipped with a double crystal monochromator (DCM), allowed tuning the excitation energy between 2.3 and 12 keV. A pass energy of 200 eV yielding an analyser resolution of 150 meV was used for all measurements. The XPS data were calibrated to C 1s reference (284.9 eV). The calibration method

was found to yield similar binding energy positions for the Cu 2p, Zn 2p, Sn 3d, and Cd 3d core levels for the CZTS reference sample for both lab-based XPS and HAXPES measurements. Except for the band bending analysis, the analysis focus on relative shifts between the core levels or with respect to the VB. The relative composition of the samples was determined by fitting the XPS and HAXPES spectra with a Voigt profile and a linear background using Igor Pro software, and considering the respective values for inelastic mean free path,[15] and photoionization cross-section[16] including the assymetry parameters of photoelectric angular distributions.[17,18] Note that the differences in transmission function of the electron energy analyzer have not been considered for the HAXPES data. However, the scope of this work is mainly to compare relative amounts between the samples. Still, the CZTS composition determined by HAXPES (at 9 keV) yielded composition ratios of Cu/Sn = 2.1, Zn/Sn = 1.07, and Cu/(Zn+Sn) = 0.9, which are not too far from the theoretical bulk composition expected

for stoichiometric Cu_2ZnSnS_4. The valence band maximum (VBM) of CZTS absorber and CdS buffer reference samples were estimated by linear extrapolation of the leading edge of the photoemission spectra.

3. Results and Discussion

3.1. Chemical Structure of the Treated CZTS Surface

To obtain information on the chemical properties of a treated CZTS surface, Al Kα XPS measurements were carried out on an AA sample, which has been etched in KCN solution, and the results are compared with a nontreated (F) CZTS sample that has also been etched in KCN. The Zn $2p_{3/2}$, Cu $2p_{3/2}$, Sn $3d_{5/2}$, O 1s, and S 2p core levels are shown in **Figure 1**. No other elements, except for some carbon contamination, are observed after the samples have been etched by KCN. In
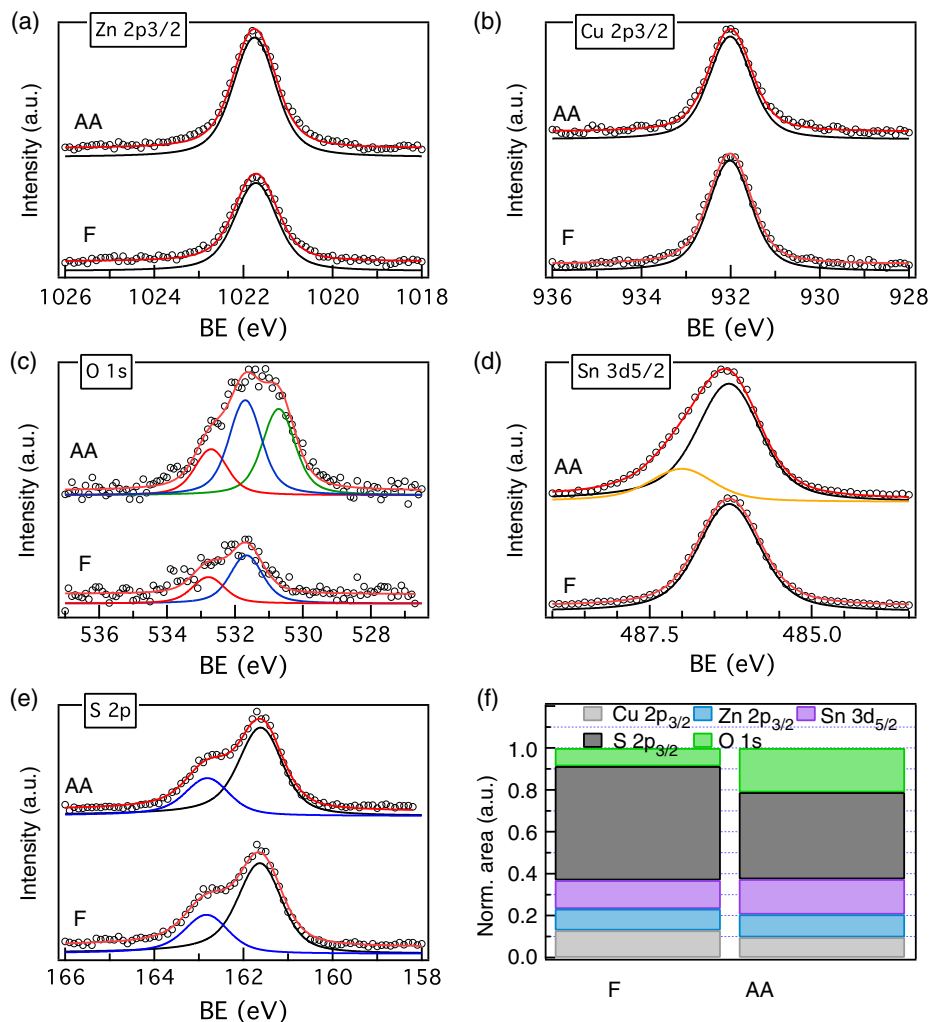

Figure 1. X-ray photoemission spectra of the freshly (F) prepared CZTS (bottom spectra) versus the AA CZTS (top spectra) absorber surfaces, recorded with an excitation energy of 1486.6 eV: a) Zn $2p_{3/2}$, b) Cu $2p_{3/2}$, c) O 1s, d) Sn $3d_{5/2}$, and e) S 2p. The spectra are displayed with the respective fits with Voigt profiles and a linear background subtracted. A composition profile is shown in (f). The peak areas were normalized such that the areas sum of all shown photoemission lines is 1 for each sample. Gray: Cu 2p, blue: Zn 2p, violet: Sn 3 d, black: S 2p, and green: O1s. The following notation is used: F = Fresh and AA = Air annealed.

addition to some intensity changes, the Zn 2p$_{3/2}$, Cu 2p$_{3/2}$, and S 2p core levels show very similar binding energies and peak shapes before and after air annealing, whereas the shape and width of the Sn 3d$_{5/2}$ core level observed after the air anneal indicates the presence of an additional chemical state around the Sn atoms. An analysis shows that two components are needed for a satisfactory fit of the spectra. Similarly, the O 1s spectrum for the AA sample shows an extra component at ≈530.5 eV (green), representative of a metal oxide (Me—O$_x$) component, likely SnO$_x$,[19] present at the CZTS surface. In addition to hydroxide (blue component at around 531.5 eV, $\Delta E = +1$ eV with respect to Me—O$_x$) and some weakly adsorbed species, probably H$_2$O (red component at around 533 eV, $\Delta E = +2.5$ eV with respect to Me—O$_x$)[20] are also observed. Similar components were also observed for the nontreated (F) CZTS sample. Some CO contribution to the O peak cannot be excluded as some weak CO$_x$ components are observed in C 1s for all samples (not shown). Several effects of an air anneal treatment of kesterite solar cells prior to buffer layer deposition have been described in the literature where the formation of SnO$_x$ has often been reported as a result of oxygen incorporation into the absorber. Also, the composition analysis shown in Figure 1f indicates that Zn and Sn concentrations increase at the surface of an AA CZTS sample as compared with the nontreated sample, similar to previous reports on the air annealing treatment of CZTS(Se).[3,4,9]

3.2. Chemical Structure of the Buffer/Absorber Interface

The surface-treated CZTS samples (AE and AA) and a nontreated (F) CZTS sample were further processed, and a thin CdS buffer was deposited. The CdS/CZTS samples were investigated by XPS at an excitation energy of 1486.6 eV. At this photon energy, the top few nanometers of a sample surface are dominating the spectra. The XPS survey spectra of the investigated CdS/CZTS samples (see Figure S1, Supporting Information) display the photoemission lines of the buffer (Cd and S) and some C and O contaminations. No additional elements were observed for the surface treated samples, and in particular, no signals from the absorber (Cu 2p and Zn 2p core levels which have the lowest inelastic mean free paths at these kinetic energies ≈1.5 nm). Some weak Sn 3d signal is observed at ≈485 eV for the non-treated (F) CZTS + CdS sample, suggesting a thinner CdS buffer layer for this sample as compared with the surface-treated CZTS samples (AE and AA). Thus, the XPS measurements show that the CdS buffer forms a complete layer, completely covering the CZTS absorber and with no evidence of pinholes. This layer has a minimum thickness of ≈6 nm for the surface-treated CZTS samples and slightly lower for the nontreated sample (thickness ≈3× inelastic mean free path of the Sn 3d photoelectrons in CdS at 1486.6 eV excitation energy).

To obtain information on the CdS/CZTS interface, HAXPES measurements were carried out and Figure S2, Supporting Information, shows the HAXPES survey spectra of the investigated CdS/CZTS sample series recorded using 3 keV photon energy. Already at this energy, all of the Cd, Cu, Zn, Sn, and S photoemission lines are present indicating that the CdS layer thickness is below 12 nm (3× inelastic mean free path of the Sn 3d photoelectrons in CdS at 3 keV excitation energy) so that the

buffer/absorber interface is probed. The Cu, Zn, and Sn peaks decrease in intensity, whereas Cd and O signals increase with changing the surface treatment from fresh to air exposure and air anneal, and a similar C signal is observed for all samples. The S signal intensity does not change significantly between the treated versus nontreated samples, as S is found in both CdS and CZTS. In addition, some weak fluorine signal just below 700 eV is observed for all samples and is likely due to contamination from the KCN solution which is used in common for different CZTS samples in our laboratory, where some of these contained F. No other signals were observed for the investigated samples. For comparison, Figure S2, Supporting Information, also shows the HAXPES spectra recorded for the CZTS and CdS reference samples. As expected, the reference samples show signals originating from the absorber (CZTS) or buffer (CdS) and some traces of carbon and oxygen.

The corresponding high-resolution spectra of individual core levels for the investigated CdS/CZTS samples and the respective peak fits are shown in **Figure 2**. The spectra are fitted with a linear background and Voigt profiles using the same relative Gaussian and Lorentzian widths for a particular line. Please note that the core-level shifts observed between the nontreated (F) versus treated (AE and AA) samples indicated with the dashed line are likely due to workfunction effects linked to a band bending observed for the nontreated sample and will be discussed more in the following paragraphs.

In agreement with the survey spectra, an intensity decrease in the peaks from CZTS and an increase in the Cd signal can be observed for the surface-treated (AE and AA) CZTS samples as compared with the nontreated (F) sample. This is likely due to a thicker buffer layer or Cd-overlayer. Also the O 1s signal increases for the surface-treated samples which is attributed to O incorporation during the surface treatment or during the buffer layer deposition. The measured relative binding energy shifts of the absorber core levels for the CdS/CZTS samples were compared with CZTS reference sample and also as reported in previous studies,[21–23] and good agreement was obtained. The XPS analysis supports that Cu, Zn, Sn, and S exist as Cu$^+$, Zn^{2+}, Sn^{4+}, and S^{2-}, respectively, in all samples, the expected oxidation states of these elements in CZTS. However, a more detailed analysis revealed that some of the core levels for the CdS/CZTS surface-treated samples show some line shape changes, such as Cd 3d and Sn 3d which showed a weak broadening upon applied surface treatment.

To obtain insights into how the surface treatment influences the chemical properties at the CdS/CZTS interface, the spectra of each individual core level were compared for the investigated samples. For an easier comparison, and to be able to identify any changes of the line shape, the photoemission spectra are normalized to the maximum intensity and aligned to the same binding energy position of the main peaks for the CZTS and CdS reference samples after subtracting a linear background. The same relative shifts between samples are observed for all core levels of the absorber material. Moreover, we found that the spectral shapes of Cu, Zn, and S lines do not change with the surface treatment and are identical to the CZTS reference (not shown), suggesting that there is no major change in the chemical composition as a result of surface treatments and
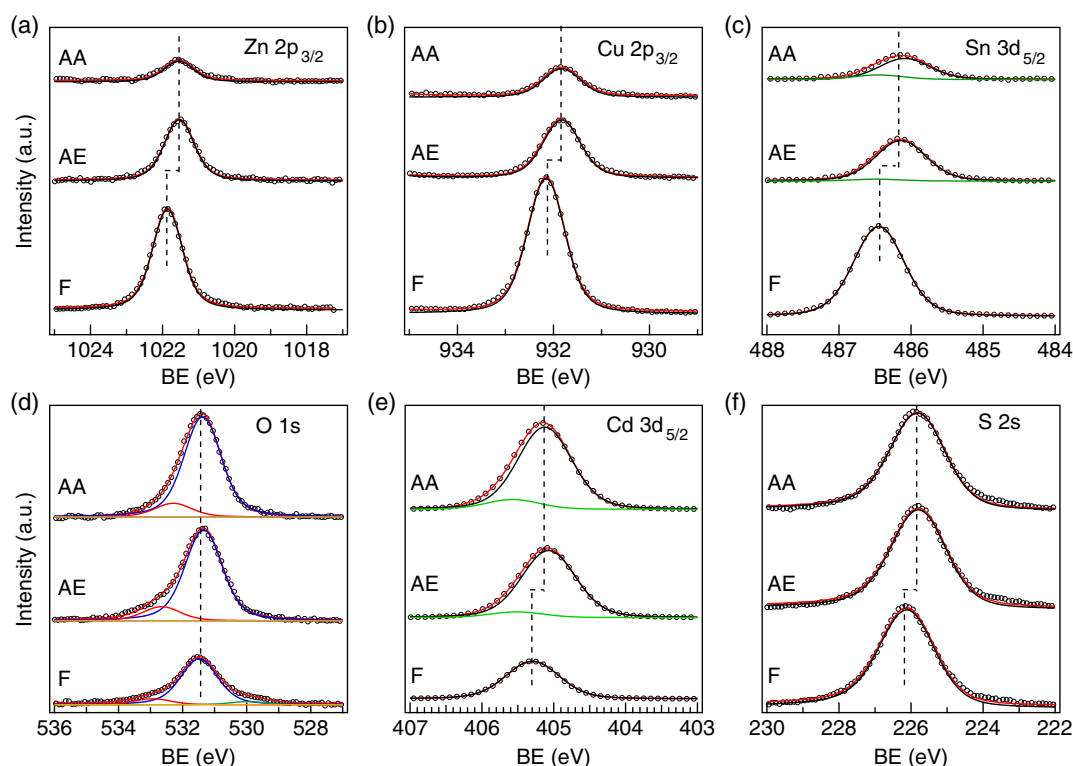
ADVANCED
SCIENCE NEWS
www.advancedsciencenews.com

physica
pssb
status solidi

www.pss-b.com

Figure 2. HAXPES data of CdS on F (bottom spectra), AE (middle spectra), and AA (top spectra) CZTS samples, recorded with an excitation energy of 3 keV: a) Zn $2p_{3/2}$, b) Cu $2p_{3/2}$, c) Sn $3d_{5/2}$, d) O 1s, e) Cd $3d_{5/2}$, and f) S 2s. The spectra are displayed with the respective fits with Voigt profiles and a linear background subtracted. Vertical dotted lines were added to facilitate the observation of binding energy variations between the samples—see text for details. The following notation is used: F = Fresh, AE = Air exposed, and AA = Air annealed.

CdS deposition. However, some slight changes in the peak shape are observed for the Sn, Cd, O, and C lines.

The peak-height-normalized and background corrected Sn $3d_{5/2}$ and Cd $3d_{5/2}$ core-level spectra for the investigated CdS/CZTS samples are shown in **Figure 3**a,b. The spectra reveal some weak broadening with the applied CZTS surface treatment as compared with the nontreated (F) sample and reference samples (CZTS or CdS references), indicating the presence of more than one chemical states around these atoms. The spectra of the non-treated (F) sample are the narrowest (FWHM(Sn 3d) = 0.82 eV, FWHM(Cd 3d) = 0.87 eV) with a similar shape as the CZTS or CdS reference samples, whereas the spectra broadens slightly for the AE sample (FWHM(Sn 3d) = 0.84 eV and FWHM(Cd 3d) = 0.92 eV) and even more for the AA CZTS + CdS sample (FWHM(Sn 3d) = 0.87 eV and FWHM(Cd 3d) = 0.95 eV). The respective fits for the AA sample are shown in Figure 3 for Sn $3d_{5/2}$ (c) and Cd $3d_{5/2}$ (d) core levels. Both the Cd and Sn 3d spectra can be represented by two components. This may indicate that both Cd and Sn have some additional chemical state in addition to the Cd- or Sn-sulfide species present in the CdS and CZTS. The binding energy difference between the two components is around 0.4 eV for both Sn 3d and Cd 3d core levels.

We tentatively attribute the small peak in Sn 3d core level to SnO_x interlayer species, whereas the main peak represents the kesterite absorber species (Sn-sulfide), similar to the soft XPS results shown in Figure 1. A similar component has previously been observed in the Sn $3d_{5/2}$ core level and was assigned to be

due to the existence of SnO_2 on the surface of CZTS. However, the surface SnO_2 was shown to be etched by aqueous ammonia during CBD process of CdS deposition.[2] In a related work, Sardashti et al.[4] showed that the dilute ammonium hydroxide, which is present in the CdS deposition bath solution and also known for dissolving oxides,[9] does not remove the SnO_x at the grain boundaries within the CZTSSe film. In particular, the presence of SnO_x at the grain boundaries, formed after annealing the bare absorber in air, is found to correlate with high device performance and is proposed to passivate grain boundaries recombination sites in CZTSSe photovoltaic devices. The fact that, in this work, the SnO_x component is still present in the Sn 3d core-level spectra for the surface-treated samples after the CBD process, and even after the KCN treatment prior to the CBD, may indicate that the formed SnO_x species are located at the grain boundaries and are thus not removed upon buffer layer growth. However, with the analysis spot of $20 \times 80\,\mu m^2$ and limited penetration depth (≈ 12 nm below the CdS surface) used here, grain boundaries versus CZTS surface area are not resolved directly and thus, we cannot for sure say that the observed SnO_x is located within the grain boundaries. We thus suggest that SnO_x is located at the surface and at the grain boundaries of the CZTS surface.

For the Cd 3d core level, the shoulder on the high binding energy side that is more pronounced for the samples that underwent a surface treatment may also indicate the formation of Cd—O_x species. However, several species have been proposed
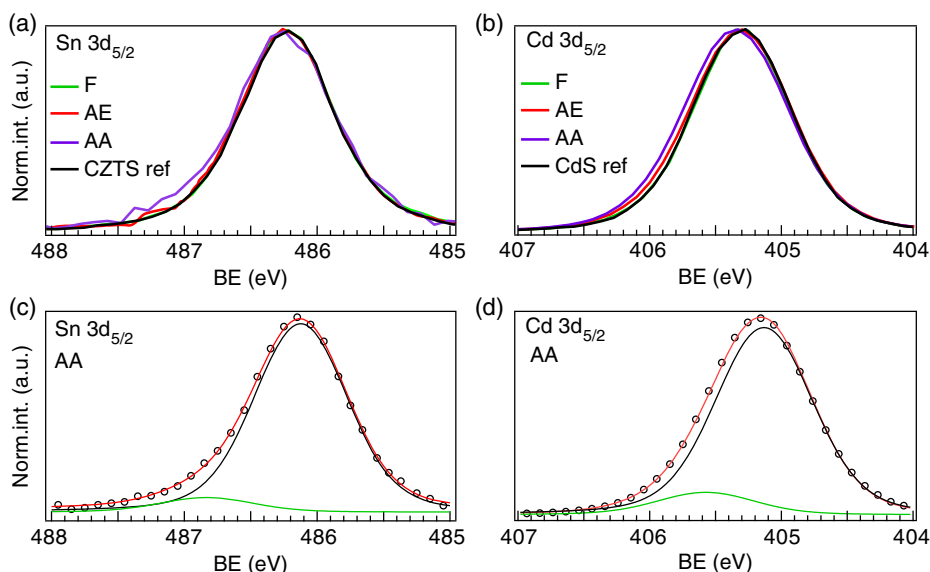
Figure 3. Evolution of the a) Sn $3d_{5/2}$ and b) Cd $3d_{5/2}$ core-level spectra recorded with and excitation energy of 3 keV for the investigated CdS/CZTS samples exposed to different surface treatments. The spectra are peak-height-normalized, background corrected, and aligned to the same energetic position of the main peak for the reference samples (CZTS for Sn 3d or CdS for Cd 3d). The respective fits with Voigt profiles and the linear background subtracted for the AA sample are shown for c) Sn $3d_{5/2}$ and d) Cd $3d_{5/2}$. The following notation is used: F = Fresh, AE = Air exposed, and AA = Air annealed.

to be present in the CdS film with similar binding energies in Cd 3d, such as CdO, Cd—CO$_3$, and Cd(CO)$_2$.[24] More information is expected to be obtained from O 1s and C 1s core levels discussed in the following paragraphs.

The corresponding O 1s and C 1s core levels of the investigated samples are shown in **Figure 4**a,b together with the respective fits for the AA sample (Figure 4c,d). For the O 1s line, the air

anneal treatment of CZTS prior to CdS deposition results in some intensity decrease at the high binding energy side of the main peak. The line shape of the O 1s is very similar for the non-treated (F) and AE samples.

Several components are clearly visible in the C 1s spectra. The main peak is assigned to hydrocarbon (C—C, C—H ≈284.9 eV), and the other peaks are attributed to oxidised forms of carbon,
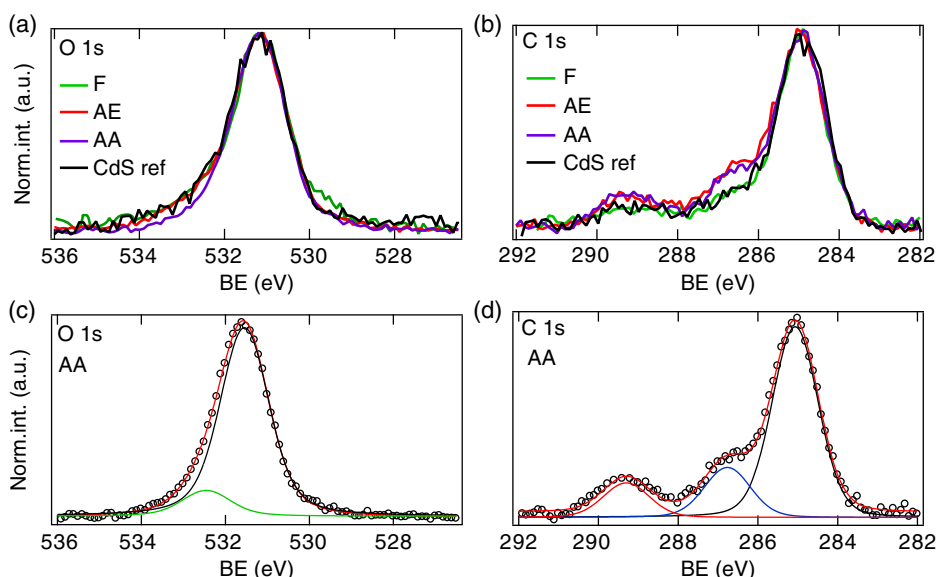

Figure 4. Evolution of the a) O 1s and c) C 1s core-level spectra recorded with and excitation energy of 3 keV for the investigated CdS/CZTS samples exposed to different surface treatments. The spectra are peak-height-normalized, background corrected, and aligned to the same energetic position of the main peak for the CdS reference sample. The respective fits with Voigt profiles and the linear background subtracted for the AA sample are shown for b) O 1s and d) C 1s. The following notation is used: F = Fresh, AE = Air exposed, and AA = Air annealed.

which are usually detected (286–288 eV [C—O(H) and HCOO and 288–289.5 eV [CO_2 and CO_3]),[24] for simplicity denoted here as CO_x. While a relatively constant hydrocarbon signal intensity observed for the different sample points to its surface adsorption during sample handling, the increasing intensity of oxidized forms of carbon for the surface-treated samples suggests its incorporation into the buffer layer. Formation of Cd—CO_3 has previously been reported for CdS deposition on $CuInSe_2$,[25] and the reported energy difference between the C1s CO_3 component and Cd $3d_{5/2}$ of 116.8 eV fits very well with our study. This may suggest that Cd—CO_x formation can take place during the buffer layer deposition of a surface-treated CZTS and is likely to contribute to the small component observed in Cd 3d discussed earlier.

Regarding the O 1s spectrum of the AA sample, two contributions were required for a satisfactory description of the fitted spectra. Comparing the binding energies of the O 1s components relative to the Cd 3d core level with values from the literature,[26] the two components for the AA sample can be assigned to hydroxide (blue component at around 531.5 eV) and adsorbed H_2O (green component at around 532.5 eV). Because CdS is deposited onto the CZTS via a wet-chemical deposition route, Cd—OH species are not unexpected. The high binding energy component has also previously been assigned to –OH species on different sites in CdS. The decrease in the high binding energy component for the AA sample as compared with the AE or fresh (F) samples supports the assignment of adsorbed H_2O of this component as water is likely to desorb at these temperatures. Thus, water may adsorb on the surface of CZTS prior to CdS deposition and can be removed by the air anneal treatment. The strong component at ≈531.5 eV may also be due to adsorbed O or C species[24,25,27,28] and $\Delta E = 126.3$ eV (between the main O 1s component and Cd $3d_{5/2}$ line) for the surface-treated samples corresponds well with the reported value for Cd—CO_3.[25] As CO_x species are visible in C 1s spectra, it is possible that part of the main peak in O1s is due to the formation of CO_x, especially as the CO_x species in both C 1s and O 1s increase simultaneously for the surface-treated samples, whereas the formation of Cd—OH species cannot be excluded. However, the O 1s spectrum for the nontreated (F) sample shows a slightly lower energy separation between the main O 1s component and Cd $3d_{5/2}$ line ($\Delta E = 126.2$ eV), which fits well with the reported value for hydroxide bonds.[26] Still, the weak component around 530 eV for the nontreated sample (F) cannot be explained at this moment. The results provide the evidence of preferential Cd—CO_x growth at the CdS/CZTS interface during the CdS deposition on a surface-treated CZTS and possible Cd—OH and adsorbed H_2O species as well, while mostly hydroxides are observed to form along with CdS during the CBD process on a nontreated (F) CZTS.

To support the assumption of formation of SnO_x and Cd—CO_x, Cd—OH species on the surface-treated samples, we looked into the thermodynamic data for compounds involving Cd, O, OH, C, and Sn, which can form on the CZTS, as shown in **Table 2**. The most negative Gibbs free energy of formation among the suggested compounds are SnO_2, Cd(CO)$_2$, Cd—CO_3, $CdSO_4$, and CdF_2. As we do not see any evidence of sulfate formation from the S core level, and the F contamination is expected to be very low, we suggest that mainly SnO_2 and Cd—CO_3/

Table 2. Standard molar Gibbs energy of formation at 298.15 K in kJ mol^{-1} for selected Cd and Sn compounds. Data taken from Engineering ToolBox website and the Handbook of Chemistry and Physics by Lide.[29]

Compound	ΔG_0
SnO	−256.9
SnO_2	−519.7
SnS	−98.3
CdO	−228.4
Cd(OH)$_2$	−473.6
CdS	−156.5
$CdCO_3$	−669.4
$CdSO_4$	−822.7
CdF_2	−700.4

Cd—$(OH)_2$ are formed at the CdS/CZTS interface for the surface-treated samples (AE and AA), whereas the nontreated (F) sample is expected to contain more of the hydroxide components within the buffer. However, it cannot be excluded that other species are present on the investigated samples, which are not included here.

To compare the influence of the surface treatment of CZTS and subsequent CdS buffer layer growth, XPS intensity changes have been compared for the investigated CdS/CZTS samples. The attenuation behavior of the different core levels recorded using an excitation energy of 3 keV is shown in **Figure 5**a. The peak areas were normalized such that the areas sum of all shown photoemission lines is 1 for each sample. Please note that the overall peak areas have been considered in Figure 5a and not the deconvoluted components of each core level (i.e., different chemical states). The absorber-related core-level intensities decrease with changing the surface treatment from nontreated (F) to AE and AA because of the attenuation by the increasingly thick buffer layer or Cd overlayer. The slight increase in the O and C intensites after the surface treatment of CZTS suggests not only a surface adsorption but also their possible incorporation into the buffer layer (in the form of Cd—CO_x/Cd—$(OH)_2$ as discussed earlier).

To investigate further how the O content correlates with the buffer layer growth, a relative composition analysis was carried out for the investigated CdS/CZTS samples and is shown in Figure 5b. An increase in the Cd and O contents as a function of surface treatment of the absorber is observed. The trend in O content is very similar to that of Cd content, i.e., the intensity increases with the surface treatment (F < AE < AA). The fact that O 1s peak intensity vary with the surface treatment and also with the Cd content may likely indicate O incorporation during the CBD process as also supported by the XPS data of CdS reference sample (not shown). This is in agreement with the results showing the formation of Cd—CO_x and Cd—OH species during the CBD process. However, a deeper O-containing layer for the treated samples cannot be excluded (below the CdS/CZTS interface). To investigate the presence of a such layer, we have repeated the XPS measurements at 9 keV incident photon energy. At such high energy, a large part of CZTS, below the CdS buffer layer (down to a probing depth of about 30 nm) is probed.
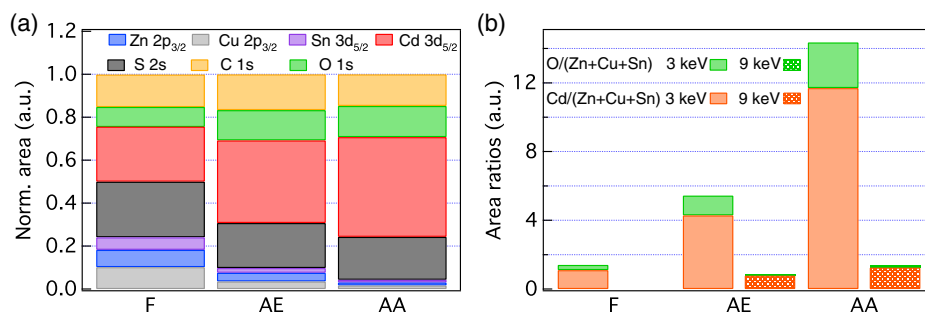
Figure 5. a) Evolution of the Zn 2p$_{3/2}$, Cu 2p$_{3/2}$, Sn 3d$_{5/2}$, Cd 3d$_{5/2}$, S 2s, C 1s, and O 1s core-level spectra for the investigated CdS/CZTS samples exposed to different surface treatments at an excitation energy of 3 keV. The peak areas were normalised such that the areas sum of all shown photoemission lines is 1 for each sample. b) Relative composition analysis for the CdS/CZTS sample series as calculated from the HAXPES data. The results are shown for both 3 keV and 9 keV measurements. The following notation is used: F = Fresh, AE = Air exposed, and AA = Air annealed.

The HAXPES results of the investigated CdS/CZTS samples at 9 keV are shown in Figure S3 and S4, Supporting Information. The HAXPES spectra at 9 keV for the surface-treated samples are very similar to the CZTS reference, as well as the measurements carried out at 3 keV. A widening of the Cd 3d$_{5/2}$ core level, similar to the measurements carried out at 3 keV, is observed for the surface-treated samples as compared with the CdS reference (FWHM[Cd 3d] increasing by ≈0.05 eV), whereas no clear change of the peak shape is observed for Sn 3d$_{5/2}$ core level, likely because the Sn 3d signal at 9 keV is dominated by the photoemission from CZTS (**Figure 6**). In addition, the more bulk-sensitive 9 keV spectra show clear differences in the O 1s core level (**Figure 7**) as compared with the 3 keV spectra (Figure 2) with the appearance of a Me—O$_x$ component at 530.5 eV in addition to the strong Me—CO$_x$/Me—OH peak observed for the measurements carried out at 3 keV (main component). This observation would suggest the presence of Me—O$_x$ species for the treated

samples deeper in the film which are not being removed upon KCN treatment. Even though, from the HAXPES spectra recorded at 9 keV photon energy, it is not clear to which absorber elements the O binds to, the soft X-ray measurements presented in Figure 1 show the formation of SnO$_x$ which is not being removed upon KCN etching or by ammonia solution from the CBD deposition. The fact that such species are not visible in the O 1s spectra at a lower probing depth (3 keV) may indicate that the SnO$_x$ species located at the surface of the CZTS may react with CdS during the CBD process and thus mostly the SnO$_x$ deeper down in the film are left after the buffer layer deposition.

In addition to the spectral shapes and attenuation behavior of the different core levels discussed earlier, some variations in the binding energy values are observed between the investigated samples. A summary of the absorber- and buffer-related core-level shifts of the investigated CdS/CZTS samples with respect
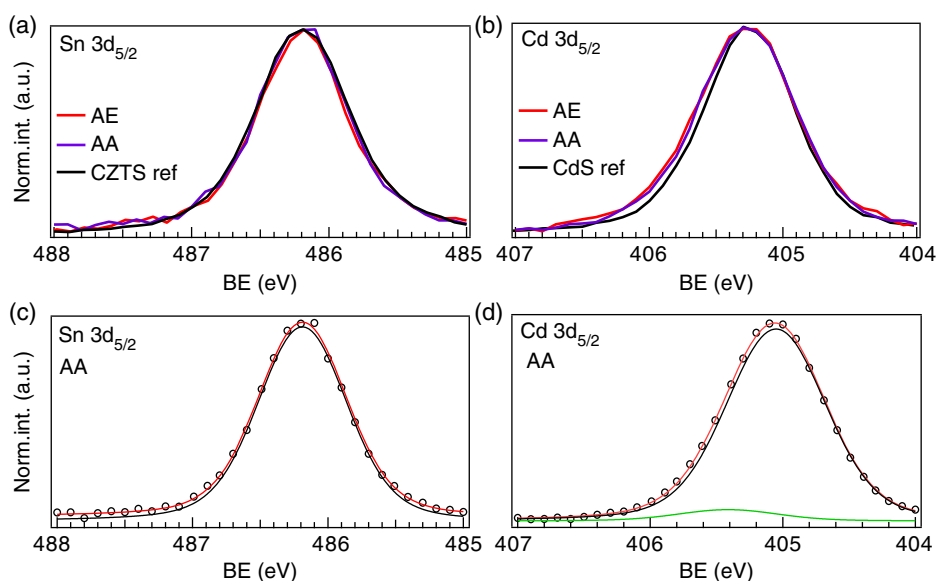

Figure 6. Evolution of the a) Sn 3d$_{5/2}$ and b) Cd 3d$_{5/2}$ core-level spectra recorded with and excitation energy of 9 keV for the investigated CdS/CZTS samples exposed to different surface treatments. The spectra are peak-height-normalized, background corrected, and aligned to the same energetic position of the main peak for the reference samples (CZTS for Sn 3d or CdS for Cd 3d). The respective fits with Voigt profiles and the linear background subtracted for the AA sample are shown for c) Sn 3d$_{5/2}$ and d) Cd 3d$_{5/2}$. The following notation is used: AE = Air exposed, and AA = Air annealed.
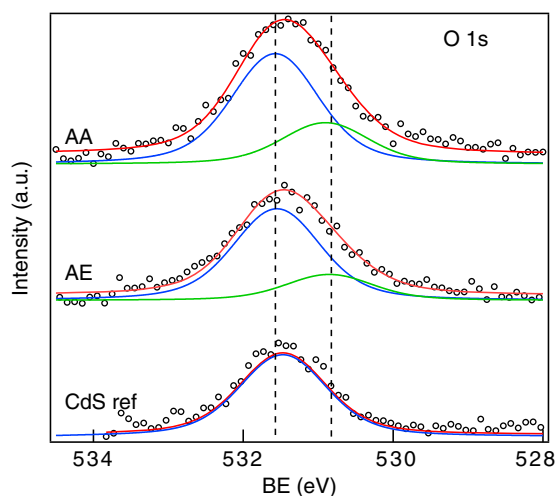
Figure 7. O 1s HAXPES data of CdS reference sample (bottom spectrum), and CdS on air exposed (middle spectrum), and AA (top spectrum) CZTS samples, recorded with and excitation energy of 9 keV. The spectra are displayed with the respective fits with Voigt profiles and the linear background subtracted. The following notation is used: AE = Air exposed and AA = Air annealed.

to the CZTS and CdS reference samples is shown in Table S1, Supporting Information. The shifts are calculated from the raw spectra as differences between the respective core level and C 1s, assuming that the same C species are present in all investigated samples. No other calibration method was available to investigate such an effect. Note that, the experimental uncertainty for all stated binding energies is 0.15 eV. For the nontreated (F) CZTS surface, the absorber core levels shift toward higher binding energies with CdS deposition. All core levels shift with the same amount, suggesting that these shifts are because of band bending rather than to chemical shifts. Thus, the absorber core level shifts for the nontreated (F) sample indicate a downward band bending as expected for the energy levels of a p-type semiconductor (CZTS) when brought into contact with an n-type material (CdS). For the treated CZTS samples (AE and AA), the fact that the absorber core levels do not shift (note that, −0.1 eV is within the experimental uncertainty of the method) toward higher binding energies with CdS deposition, points to Fermi-level pinning presumably due to high density of defects at the absorber surface and/or buffer/absorber interface. This is not too surprising as the photoemission results discussed earlier showed evidence of SnO_x and $Cd-CO_x$ species within the CZTS surface grain boundaries and at the CdS/CZTS interface.

3.3. Influence of Applied Surface Treatment on CdS Growth and Suggested Model

To summarize the results so far, we have evaluated the photoemission line intensities, their attenuation behavior upon buffer layer deposition as a function of surface treatments, their peak positions, and their spectral shapes. We find that the spectral shape of some of the absorber and buffer peaks change upon

applied surface treatment and subsequent buffer layer deposition pointing to the formation of SnO_x and $Cd-CO_x$ species. Following the evolution of the core levels with excitation energy (and thus with probing depth), some clear differences are observed in the O 1s core level suggesting that the SnO_x formed during the surface treatment is located at and below the CdS/CZTS interface, likely at the surface and grain boundaries within the CZTS surface, whereas $Cd-CO_x$ forms at the buffer/absorber interface and $Cd-OH$ is observed at the interface and within the buffer layer. Also, the surface treatments seem to influence the CdS growth mechanism as an increasingly thick CdS overlayer is observed for the surface-treated samples as compared with the nontreated sample. A possible explanation for this may be the difference in the incubation/nucleation period in the very first stages of the CBD process. We suggest that this incubation period may be reduced for the surface-treated CZTS samples which may lead to a thicker CdS layer growth. Another suggestion may be the Cd interaction with SnO_x layer during the CdS deposition. In the very first stages of CBD (during which no S is released from the thiourea ≈1 min), SnO_x may provide O for the interaction with Cd forming $Cd-O$ bonds (an intermixed $Cd-O_x$, $Sn-O_x$ layer at the CdS/CZTS interface). This will also give rise to an increased amount of Cd as observed for the surface-treated samples. In both cases, the formation of $Cd-CO_x$ is possible. With the available data, it is difficult to distinguish between the CdS ($+Cd-CO_x$, $-OH$) and $Cd-O+CdS$ ($+Cd-CO_x$, $-OH$) on top of the CZTS, and the buffer deposited on the CZTS is thus denoted here as CdS-overlayer. However, the O 1s data discussed earlier support the interaction of the CZTS surface oxygen species with CdS and thus, the second possibility, i.e., Cd interaction with SnO_x, is a more plausible explanation. The main conclusions regarding the formation of different interface species allow us to propose a model for the chemical structure of the CdS/CZTS interface of surface treated CZTS samples, as shown in **Figure 8**b. It cannot be excluded that other features may be formed during the surface treatment of CZTS and subsequent CdS deposition, which, however, are not probed by the methods used in this work. Note that, the same interface layers are formed for both surface-treated samples (AE and AA), the main difference between them being a thicker CdS-overlayer for the AA sample. No interface layer has been observed for the nontreated sample (F) and subsequent CdS deposition in this work (Figure 8a).

3.3.1. Electronic Structure of the Buffer/Absorber Interface

To obtain more information about the electronic band alignment at the interface between the CdS buffer and CZTS absorber, the VBO, i.e., the relative alignment of the VB at the interface between CdS and CZTS, has been measured in the set of investigated samples by HAXPES. The VB spectra of the CdS/CZTS samples are composed of a mixture of the VBs of CdS and CZTS, and can be affected by various interface effects (e.g., Fermi-level pinning, defects, and lattice mismatch). Among the interface properties, the band offset is one of the most important parameters in a solar cell because it influences the transport and recombination of carriers. A downward shift of the VBM, among other things, is expected to lead to a reduced interface recombination
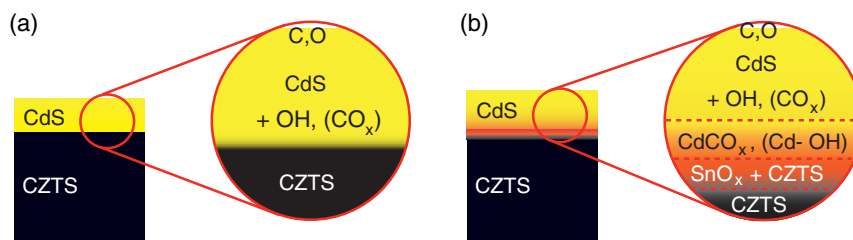
Figure 8. Schematic representation of the chemical structure of the CdS/CZTS interface for the a) nontreated (F) CZTS and b) a surface-treated (AE and AA) CZTS. See text for details.
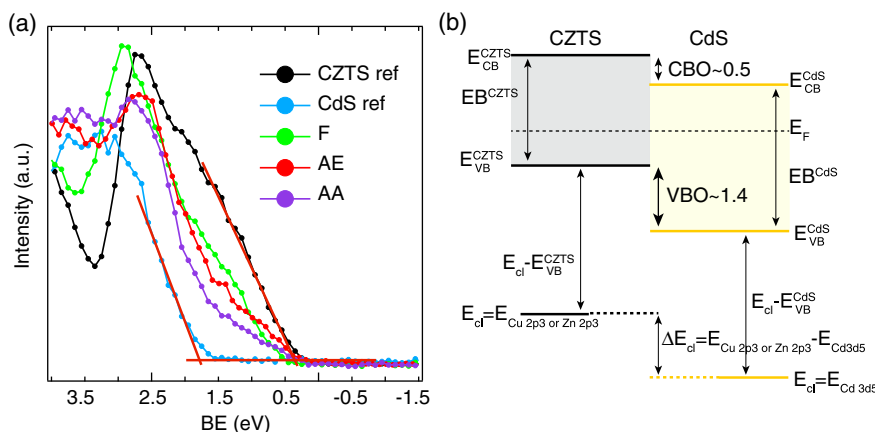

Figure 9. a) XPS VB spectra of the investigated CdS/CZTS samples recorded with 3 keV photon energy together with the VB spectra recorded from the CdS and CZTS reference samples. The following notation is used: F = Fresh, AE = Air exposed, AA = Air annealed. b) Schematic illustration of the band allignment at the CZTS/CdS heterojunction showing the measured energy values as well as the determined VBO and estimated CBO for the surface-treated CZTS samples (AE and AA). Similar results were obtained for the nontreated (F) sample (Table 3).

rate in solar cells with n + p junctions, i.e., where the p-type absorber surface is inverted.[30] To determine the VBO of the CdS/CZTS heterojunction, we measured VB spectra of thick CZTS and CdS films, as shown in **Figure 9**a. From the calibrated spectra, the VB edges are determined to be 0.3 ± 0.15 and 1.7 ± 0.15 eV for CZTS and CdS, respectively, by a linear extrapolation of the leading edge to the extended baseline. This implies that the CZTS surface is not inverted before buffer deposition. To determine the VBO of the CdS/CZTS heterojunction, the core levels of the thick CZTS and CdS films, as well as the CdS/CZTS heterojunction, were measured as reference levels and as previously shown in Figure 2.

The VBO of the CdS/CZTS interface was calculated by the Krauts formula,[31] as also shown in Figure 9b

$$VBO = (E_{cl} - E_{VB})_{absorber} - (E_{cl} - E_{VB})_{buffer} - \Delta E_{cl} \quad (1)$$

where E_{cl} is the binding energy of a core level (Cu 2p or Zn 2p) in the absorber, E_{VB} is the VBM of either the CZTS or CdS references measured by HAXPES, and ΔE_{cl} is the energy difference between a core level in the absorber and a core level in the buffer measured for the CdS/CZTS samples. The first two terms give the relative binding energy difference between a core level and the VB in the absorber and buffer references, respectively. The last term gives the relative binding energy between absorber and buffer core levels measured at the

CdS/CZTS interface by HAXPES. It is assumed that the VBM of the CZTS or CdS do not vary too much in the bulk versus the near surface region of the material. The determined values for the VBO of the investigated CdS/CZTS samples are shown in **Table 3**.

To estimate the conduction band offset (CBO) of the CdS/CZTS interface, the bandgaps of the CdS/CZTS sample series are determined from quantum efficiency measurements. The results (**Figure 10**a,b) show a constant CZTS bulk bandgap (EB) value of 1.5 ± 0.05 eV for all investigated CdS/CZTS samples. The bandgap has been extracted using a linear extrapolation of the leading edge spectrum, as shown in Figure 10b and discussed more in the study by Larsen et al.[32] A constant value of 2.4 eV was used for the CdS bulk bandgap as previously reported.[2] The CBO can then be determined from the VBO, and the optical bandgap and the results are shown in Table 3 (see Figure 9b for a band alignment illustration). It is assumed that the electronic bandgaps of the CZTS or CdS is the same as the optical bandgaps of these materials do not vary too much in the bulk versus the near surface region of the material.

$$CBO = EB_{absorber} - EB_{buffer} - VBO \quad (2)$$

A cliff-like CBO of the heterojunction interface is determined for all investigated samples (≈ 0.4–0.5 eV), independent of

Table 3. Photovoltaic properties of the solar cells fabricated from the set of samples discussed in this work (cell structure: Al:ZnO/CdS/CZTS/Mo/SLG). (η: conversion efficiency [%], J_{sc}: short-circuit current density [mA cm^{-2}], V_{oc}: open-circuit voltage [V], FF: fill factor [%]), VBO: valence band offset and CBO: conduction band offset at the buffer/absorber interface [eV].

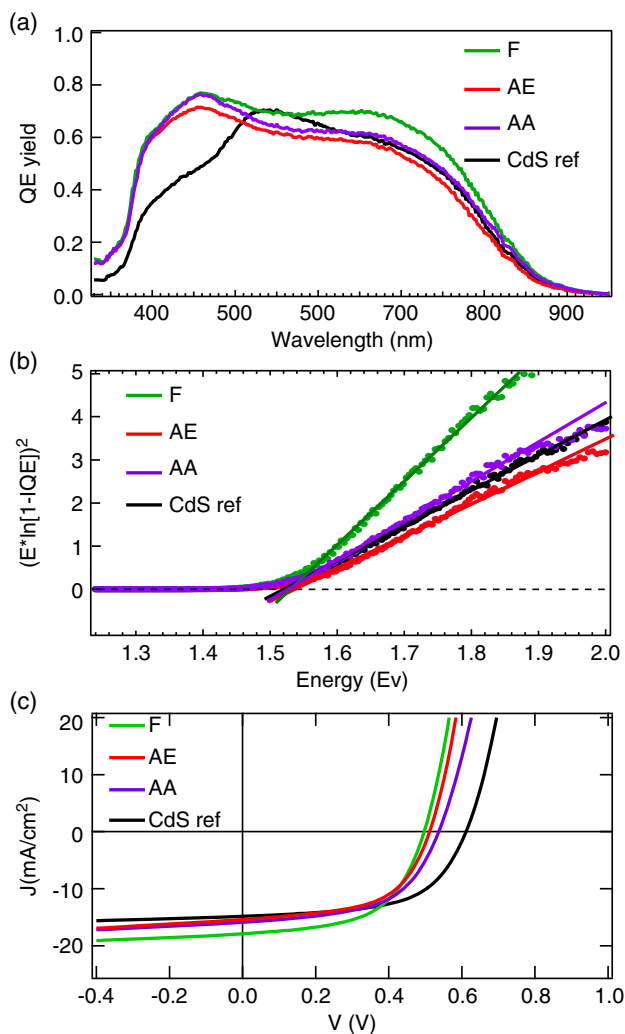| Sample ID	Comment	η	J_{sc}	V_{oc}	FF	VBO	CBO
CdS ref	Reference thick CdS on fresh CZTS	5.31	14.8	0.610	58.6	–	–
F+CdS	Fresh CZTS + thin CdS	4.98	17.9	0.496	56.2	−1.3	−0.4
AE+CdS	24 h AE CZTS + thin CdS	4.46	15.4	0.511	56.8	−1.4	−0.5
AA+CdS	AA CZTS + thin CdS	4.72	15.9	0.536	55.5	−1.4	−0.5
AA+CdS ref	AA CZTS + thick CdS[3]	6.8	19	0.623	57.6	–	–

Figure 10. a) Quantum efficiency measurements of the investigated CdS/CZTS samples. b) Determination of the bandgaps from a linear extrapolation of the leading edge in the spectrum. c) J–V characteristics of the best cell from reference CZTS device and surface-treated CZTS devices. The following notation is used: F = Fresh, AE = Air exposed and AA = Air annealed.

good agreement was found with some previous works,[34] the CBO values calculated in this work show an increased cliff compared with other previously reported values. Variations in the CBO value at the CZTS/CdS interface have previously been reported. Crovetto and Hansen have analyzed the possible mechanisms in detail, which can determine CBO variations.[8] Fermi-level pinning, chemical interdiffusion, etching of the absorber, or quantum confinement in the CdS seed layer for thinner films have been identified as possible mechanisms that influence the band edge position at the CZTS/CdS interface.

In particular, it is worth noting the difference in the CBO value (large cliff) as compared with the HAXPES study by Tajima et al.[2] where a flat CBO was determined. The difference could be caused by the interface behavior due to the process conditions and differences in the composition of the CZTS layer, but also due to differences in the evaluation of the CBO. There is a large difference already in the VBO value between this study and Tajima's work (1.3 vs 1.0 eV). Tajima et al. presented a direct measurement of the VBO at the CdS/CZTS interface by fitting of the VB HAXPES spectra, whereas in our work, an indirect estimation of VBO was made using extrapolation of the HAXPES signal to determine VBM of CZTS and CdS. In addition, the used photon energy is different in the two studies (3 vs 8 keV) which implies that VBO is determined at different depths for similar CdS layer thicknesses. Differences in CZTS bulk bandgap between the two studies (1.53 vs 1.4 eV) measured by external quantum efficiency may also contribute to the observed CBO differences.

However, the aim of the band alignment study presented in this work is to compare relative changes between the investigated samples. A comparison between the treated versus nontreated samples shows a negligible difference in the calculated CBO value (0.1 eV), with the assumption of a constant buffer bandgap. This indicates that the band alignment is not significantly altered by a surface treatment of CZTS for a thin CdS buffer layer. It cannot be excluded that interface bandgaps may be different due to interface-related phenomena such as interdiffusion during the surface treatments.[35]

Even more, it shall be noted here that this model is for an abrupt CZTS/CdS buffer interface, but, as shown in Figure 8b, additional interface components come into play for the surface-treated samples. The formation of some thin interlayers between CZTS and CdS, such as SnO$_x$ or CdO$_x$, may modify the band alignment with CZTS and CdS layers and could thus impact interface recombination through passivation. The band

surface treatment. There is a consensus in the literature that, for pure sulfide CZTS, the experimentally determined CBO values at the CdS/CZTS interface are negative (cliff).[33] Even though a

ADVANCED
SCIENCE NEWS
www.advancedsciencenews.com

physica pssb
status solidi

www.pss-b.com

alignment of such thin interlayers is difficult to probe with the used method.

3.3.2. Electrical Characterization

To verify how the findings presented earlier correlate with the device characteristics, photovoltaic cells were fabricated from half of each sample prepared and discussed earlier, and $J–V$ measurements were carried out. Figure 10c shows the $J–V$ characteristics of the best cell from reference CZTS device and surface-treated CZTS devices with a CdS buffer. The photovoltaic properties of the best solar cells for each sample are shown in Table 3. The air anneal treatment leads to an increase in V_{OC} as compared with a nontreated (F) CZTS sample+buffer (with identical CBD process) similar to the work by Larsen et al.[3] The difference in J_{SC} between the samples can be explained by the difference in parasitic absorption in the CdS as seen in the quantum efficiency measurements (Figure 10a). The nontreated (F) sample also shows highest collection for long wavelengths which could either be due to a longer minority carrier diffusion length in the bulk CZTS, or more extended space charge region. The efficiency of the presented CdS/CZTS devices is relatively low, but we would like to point out that these samples contain a thin buffer layer (<10 nm) to facilitate HAXPES analysis, much thinner than the typical thickness used in high efficiency devices (≈50–60 nm). A low efficiency has previously been reported for a thin CdS buffer layer.[2] Even though a good agreement of increased device performance for the surface-treated samples is observed for this work, the comparison with the work by Larsen et al.[3] shall only be seen as relative as, other variables, such as variations in CZTS bulk composition may influence device performance. The extent to which the formed chemical species at the buffer surface and buffer/absorber interface are related to the increase in cells efficiency upon surface treatment has to be investigated in more detail in the future. We speculate that the formation of SnO_x through a surface treatment may influence the buffer layer growth and contribute to a reduced interface recombination through passivation, which could very well have an impact on the cells performance. This is in agreement with previous reports on the efficiency enhancement of kesterite CZTS solar cells through SnO_2 interface passivation.[36]

4. Conclusions

XPS and HAXPES have been used to study the chemical and electronic properties of the absorber surface and buffer/absorber interface when a CZTS solar cell absorber was subjected to different surface treatments and subsequent CdS deposition. We find that the band alignment at the CdS/CZTS interface is not significantly altered by the applied surface treatment but chemical changes are observed at the CZTS surface and CZTS/CdS interface. A surface treatment of CZTS (elongated air exposure or short air anneal) induces a surface composition change with the formation of metal oxides, most of them being removed by a surface cleaning treatment of KCN. Still, the results provide evidence that SnO_x, located likely at the surface and within the grain boundaries of CZTS surface, is not removed by the KCN treatment, and an increasing Cd content is observed

for the surface-treated samples with identical CBD processes. Also, the results show the formation of Cd-CO$_x$ species at the Cd/CZTS interface for the surface-treated samples which may, in part, be responsible for the observed structural and chemical differences. The different CdS growth mechanism for the surface-treated samples may influence interface recombination so a reoptimization of the CdS thickness for a given surface treatment may be required.

Supporting Information

Supporting Information is available from the Wiley Online Library or from the author.

Conflict of Interest

The authors declare no conflict of interest.

[1] C. Yan, J. Huang, K. Sun, S. Johnston, Y. Zhang, H. Sun, A. Pu, M. He, F. Liu, K. Eder, L. Yang, J. M. Cairney, N. J. Ekins-Daukes, Z. Hameiri, J. A. Stride, S. Chen, M. A. Green, X. Hao, *Nat. Energy* **2018**, *3*, 764.

[2] S. Tajima, K. Kataoka, N. Takahashi, Y. Kimoto, T. Fukano, M. Hasegawa, H. Hazama, *Appl. Phys. Lett.* **2013**, *103*, 243906.

[3] J. K. Larsen, Y. Ren, N. Ross, E. Särhammer, S.-Y. Li, C. Platzer-Björkman, *Thin Solid Films* **2017**, *633*, 118.

[4] K. Sardashti, R. Haight, T. Gokmen, W. Wang, L.-Y. Chang, D. B. Mitzi, A. C. Kummel, *Adv. Energy Mater.* **2015**, *5*, 1402180.

[5] M. Neuschitzer, Y. Sanchez, T. Olar, T. Thersleff, S. Lopez-Marino, F. Oliva, M. Espindola-Rodriguez, H. Xie, M. Placidi, V. Izquierdo-Roca, *Chem. Mater.* **2015**, *27*, 5279.

[6] I. Repins, C. Beall, N. Vora, C. DeHart, D. Kuciauskas, P. Dippo, B. To, J. Mann, W.-C. Hsu, A. Goodrich, R. Noufi, *Sol. Energy Mater. Sol. Cells* **2012**, *101*, 154.

[7] Y. Ren, J. S. Scragg, M. Edoff, J. L. Larsen, C. Platzer-Björkman, *ACS Appl. Mater. Interfaces* **2016**, *8*, 18600.

[8] A. Crovetto, O. Hansen, *Sol. Energy Mater. Sol. Cells* **2017**, *169*, 177.

[9] R. Haight, X. Y. Shao, W. Wang, D. B. Mitzi, *Appl. Phys. Lett.* **2014**, *104*, 033902.

[10] J. H. Kim, S.-Y. Choi, M. Choi, T. Gershon, Y. S. Lee, W. Wang, B. Shin, S.-Y. Chung, *Adv. Energy Mater.* **2016**, *6*, 1501902.

[11] M. Bär, B.-A. Schubert, B. Marsen, S. Krause, S. Pookpanratana, T. Unold, L. Weinhardt, C. Heske, H.-W. Schock, *Appl. Phys. Lett.* **2011**, *99*, 152111.

[12] J. K. Larsen, J. J. S. Scragg, C. Frisk, Y. Ren, C. Platzer-Björkman, *Phys. Status Solidi A* **2015**, *212*, 2843.

[13] J. Lindahl, U. Zimmermann, P. Szaniawski, T. Törndahl, A. Hultqvist, P. Salome, C. Platzer-Björkman, M. Edoff, *IEEE J. Photovolt.* **2013**, *3*, 1100.

[14] D. Céolin, J. M. Ablett, D. Prieur, T. Moreno, J.-P. Rueff, B. Pilette, T. Marchenko, L. Journel, T. Marin, R. Guillemin, M. Simon, *J. Electron. Spectrosc. Relat. Phenom.* **2013**, *190*, 188.

[15] a) S. Tanuma, C. J. Powell, D. R. Penn, *Surf. Interface Anal.* **1994**, *21*, 165; b) S. Tougaard, *Quases-IMFP-TPP2M, Ver. 3.0*, QUASES-Tougard, Odense, Denmark **2016**, http://www.quases.com/products/quases-imfp-tpp2m/.

[16] J. H. Scofield, *Theoretical Photoionization Cross Sections from 1 to 1500 keV*, Technical Report, Lawrence Livermore Laboratory, Livermore, USA **1973**, https://doi.org/10.2172/4545040.

[17] J. J. Yeh, I. Lindau, *Atom. Data Nucl. Data* **1985**, *32*, 1.

[18] I. M. Band, Yu. I. Haritonov, M. B. Trzhaskovskaya, *Atom. Data Nucl. Data* **1979**, *23*, 443.

[19] L. Sun, Y. Kurosawa, T. Yoshida, Y. Suzuri, *J. Electrochem. Soc.* **2019**, *166*, B3176.

[20] J.-C. Dupin, D. Gonbeau, P. Vinatier, A. Lavasseur, *Phys. Chem. Chem. Phys.* **2000**, *2*, 1319.

[21] G. Gordillo, C. Calderon, P. Bartolo-Perez, *Appl. Surf. Sci.* **2014**, *305*, 506.

[22] M. Valdes, M. F. Pacual-Winter, A. Bruschhausen, W. Schreiner, M. Vasquez, *Phys. Status Solidi A* **2018**, *215*, 1800639.

[23] C. A. Meza Avendano, N. R. Mathews, M. Pal, F. P. Delgado, X. Mathew, *ECS J. Solid State Sci. Technol.* **2015**, *4*, P91.

[24] M. E. Maliki, J. C. Bernede, S. Marsillac, J. Pinel, X. Castel., J. Pouzet, *Appl. Surf. Sci.* **2003**, *205*, 65.

[25] C. Guillen, M. A. Martinez, C. Maffiotte, J. Herrero, *J. Electrochem. Soc.* **2001**, *148*, G602.

[26] N. Maticiuc, A. Katerski, M. Danilson, M. Krunks, J. Hiie, *Sol. Energy Mater. Sol. Cells* **2017**, *160*, 211.

[27] M. Stoev, A. Katerski, *J. Mater. Chem.* **1996**, *6*, 377.

[28] A. Kylner, A. Rockett, L. Stolt, *Solid State Phenom.* **1996**, *51–52*, 533.

[29] a) Engineering ToolBox, Standard State and Enthalpy of Formation, Gibbs Free Energy of Formation, Entropy and Heat Capacity, https://www.engineeringtoolbox.com (accessed January 2020); b) D. R. Lide, in *Handbook of Chemistry and Physics*, CRC Press, Boca Raton, FL **1998**-1999.

[30] R. Klenk, *Thin Solid Films* **2001**, *387*, 135.

[31] J. R. Waldrop, E. A. Kraut, C. W. Farley, R. W. Grant, *J. Appl. Phys.* **1991**, *69*, 372.

[32] J. Larsen, F. Larsson, T. Törndahl, N. Saini, L. Riekehr, Y. Ren, A. Biswal, D. Hauschild, L. Weinhardt, C. Heske, C. Platzer-Björkman, *Adv, Energy Mater.* **2019**, 1900439.

[33] C. Platzer-Björkman, N. Barreau, M. Bär, L. Choubrac, L. Grenet, J. Heo, T. Kubart, A. Mittiga, Y. Sanchez, J. Scragg, S. Sinha, M. Valentini, *J. Phys.: Energy* **2019**, *1*, 044005.

[34] M. Bär, B.-A. Schubert, B. Marsen, R. G. Wilks, S. Pookpanratana, M. Blum, S. Krause, T. Unold, W. Yang, L. Weinhardt, C. Heske, H.-W. Schock, *Appl. Phys. Lett.* **2011**, *99*, 222105.

[35] A. Crovetto, A. Cazzaniga, R. Bolt Ettlinger, J. Schou, O. Hansen, *Sol. Energy Mater. Sol. Cells* **2018**, *187*, 233.

[36] H. Sun, K. Sun, J. Huang, C. Yan, F. Liu, J. Park, A. Pu, J. A. Stride, M. A. Green, X. Hao, *ACS Appl. Energy Mater.* **2018**, *1*, 154.